Journal of Hazardous Materials 183 (2010) 211–217

Contents lists available at ScienceDirect

Journal of Hazardous Materials

journal homepage: www.elsevier.com/locate/jhazmat

Processing–structure–property relationships of Bi_2WO_6 nanostructures as visible-light-driven photocatalyst

Zhankui Cui [a], Dawen Zeng [a,b,*], Tengteng Tang [b], Jun Liu [b], Changsheng Xie [b]

[a] State Key Laboratory of Material Processing and Die & Mould Technology, Huazhong University of Science and Technology, Wuhan 430074, China
[b] Nanomaterials and Smart Sensors Laboratory, Department of Materials Science and Engineering, Huazhong University of Science and Technology, Wuhan 430074, China

ARTICLE INFO

Article history:
Received 16 April 2010
Received in revised form 15 June 2010
Accepted 2 July 2010
Available online 10 August 2010

Keywords:
Bi_2WO_6 nanostructures
Calcination
Visible light
Photocatalyst

ABSTRACT

QDS modified Bi_2WO_6 (BWO) nanostructures were processed by calcination at different temperatures. A strong correlation was found among the processing, structure and properties of the samples. With increasing calcination temperature from 200 °C to 500 °C, the crystallinity increased and the BWO QDS gradually disappeared from the nanostructures. Both surface area and band gap of the samples decreased. The light absorption of the samples became lower for the long-wavelength range, accompanied by a red shift of the absorption edge. The photocatalytic activity of the samples decreased after calcination at higher temperature. The competitive relations between crystallinity and surface area in affecting photocatalytic activity were discussed. The role of BWO QDS that played in enhancement of photocatalytic activity was also revealed by studying structure and property evolution of the calcined samples.

1. Introduction

Semiconductor photocatalysis has become the focus of investigations due to its potential applications for solar energy conversion and environmental purification [1,2]. Among various semiconductor oxides, the layered tungsten compounds are considered to be one important category of photocatalysts [3], such as $Na_2W_4O_{13}$ [4], $ZnWO_4$ [5] and $CdWO_4$ [6]. But most of them respond only to UV irradiation, which limits their application into practice. Recently, perovskite-like Bi_2WO_6 (BWO) has been found to have excellent photocatalytic activity under visible-light irradiation when used to decompose water dyes and indoor pollutants [7–9]. Though much effort has been devoted to reveal its unique physical and chemical properties, we still have dearth information about BWO. Thereby, it is urgent to further explore the preparation, characterization and application of this new photocatalyst.

It is well known that the properties of materials greatly depend on their structure including crystal structure and microstructure. Especially, for a specific photocatalyst, the most important factors that determine its photocatalytic activity are considered to be crystallinity and surface area [10]. Previously, much effort has been devoted to increase the crystallinity and the surface area, and most measures that were taken relate to nanotechnology [11]. Moreover, different routines for preparing and processing nanomaterials lead to different photocatalytic activity. The routines and the properties are correlated with structure of materials [12–14]. Considering BWO photocatalyst, much attention has been focused on preparation of BWO nanomaterials such as nanoparticles and nanostructures. There are only a few reports on processing-structure-property relationships of BWO photocatalysts. Calcination is a very common processing method to adjust structure and properties of materials. Here we calcined QDS modified BWO nanostructures at different temperatures and emphasized to investigate processing–structure–property relationships by observing structure–property evolution caused by calcination. We also attempted to reveal the role of BWO QDS in improving photocatalytic activity of BWO nanostructures.

2. Experiments

2.1. Preparation of samples

All reagents were of analytical grade and were used as received without any further purification. BWO nanostructures were prepared by solvothermal method. In a typical case, 0.26 g $Bi(NO_3)_3{\cdot}5H_2O$ and 0.14 g WCl_6 were dissolved in 25 ml ethylene glycol, respectively. The two solutions were mixed together under magnetic stirring for several hours at room temperature until a transparent solution was obtained. Then 0.32 g urea was added into the above solution. The solution was still transparent and was transferred into an 80 ml Teflon-lined stainless steel autoclave. The autoclave was sealed and maintained at 180 °C for 15 h and then

* Corresponding author at: State Key Laboratory of Material Processing and Die & Mould Technology, Huazhong University of Science and Technology, Wuhan 430074, China.
E-mail address: dwzeng@mail.hust.edu.cn (D. Zeng).

0304-3894/$ – see front matter © 2010 Elsevier B.V. All rights reserved.
doi:10.1016/j.jhazmat.2010.07.013

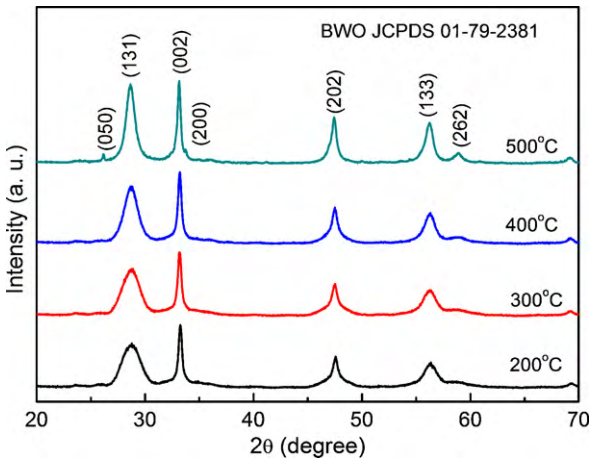

Fig. 1. XRD patterns of the samples calcined at different temperatures.

cooled to room temperature naturally. The resultant powers were filtered off and washed with absolute ethanol and deionized water for three times to remove EG and impurity ions. The samples were dried at 80 °C in air for 10 h and then calcined in the muffle furnace at 200 °C, 300 °C, 400 °C and 500 °C for 1 h. They were short for BWO-2, BWO-3, BWO-4 and BWO-5, respectively.

2.2. Characterizations

The phase and crystal structure of the samples were analyzed by means of a X'pert Pro X-ray diffractometer with Cu Kα radiation (λ = 1.5418 å) under 40 kV and 100 mA. The samples were further characterized by a Siron field-emission scanning electron microscopy (FESEM) and a JEOL transmission electron microscopy (TEM) operated at 200 KV. Brunauer–Emmett–Teller (BET) surface area of the samples were determined by a Micrometrics ASAP-2020 nitrogen adsoprtion/desorption measurement appratus. The optical properties were evaluated by studying the diffusion reflectance spectra (DRS) on a PerkinElmer Lamda-35 UV–vis spectrophotometer.

2.3. Photocatalytic activity tests

The photocatalytic activity of all the samples was measured by degradation of Rhodamine B (RhB) under visible-light irradiation using a 350 W Xe lamp with a 420 nm cut-off filter. The distance between the lamp and the reactor was 20 cm. In each experiment, 0.05 g of photocatalyst was dispersed into 100 ml 10^{-5} mol/L RhB solution ultrasonically. Before illumination, the suspensions were magnetically stirred for 60 min to ensure the establishment of an adsorption–desorption equilibrium between photocatalyst and RhB in the dark. Then the solution was exposed to visible-light irradiation under magnetic stirring. At each interval of 15 min, 3 ml of suspension was sampled and centrifuged. The solution was analyzed by a Unico-2102 spectrophotometer and the adsorption peak at 554 nm was monitored. The photocatalytic efficiency was calculated according to the following equation:

$$\text{efficiency}\,(\%) = \frac{C_0 - C}{C_0} \times 100\%$$

where C_0 and C represent the initial concentration of RhB prior to irradiation and the concentration of RhB after irradiation for in a given time, respectively.

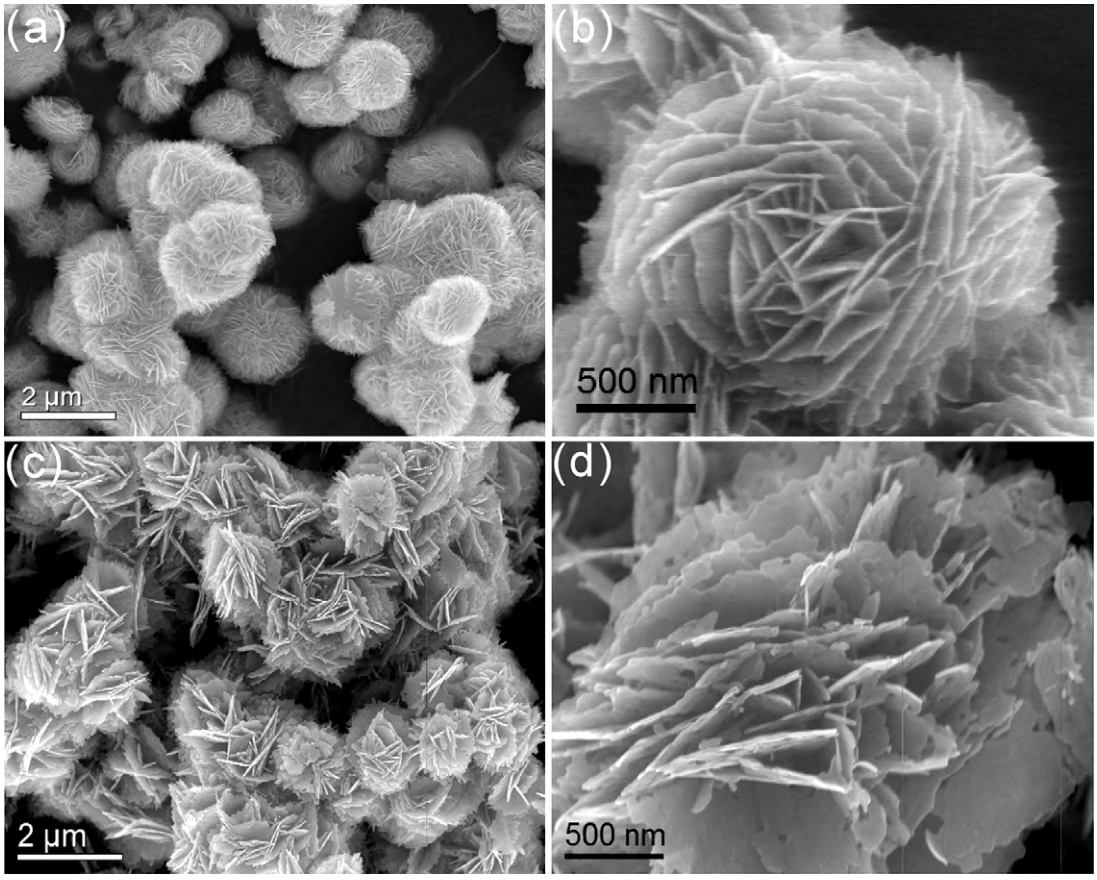

Fig. 2. SEM images of the samples calcined at 200 °C (a) and (b), and 500 °C (c) and (d).

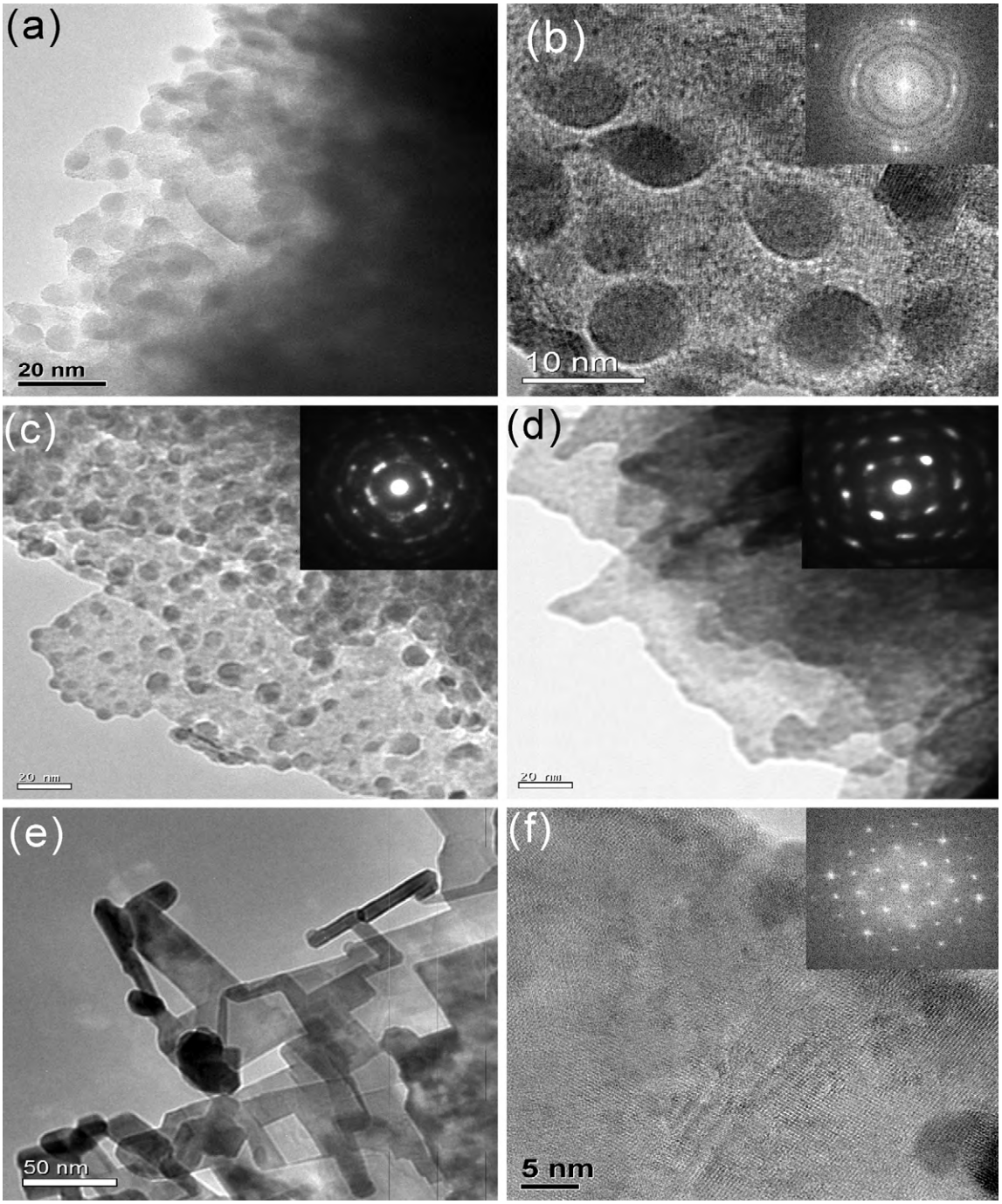

Fig. 3. TEM images of the samples calcined at 200 °C (a) and (b), 300 °C (c), 400 °C (d), and 500 °C (e) and (f).

3. Results and discussion

3.1. XRD studies

Fig. 1 shows XRD patterns of the calcined samples. From the patterns, all peaks can be assigned to orthonormal Bi_2WO_6 phase, which is consistent with JCPDS No. 01-79-2381 and no other peaks originated from impurities were found on the spectra. The peaks in the XRD spectrum of BWO-2 were broad except for the peak at 33.1 °C corresponding to (0 0 2) plane. The sharp peak indicates preferred orientation took place and the samples obtained by solvothermal route were crystalline. The broad peaks may be due to the existence of small size particles in the BWO nanostructures. With increasing calcination temperature, the peaks became stronger and sharper. At 500 °C, two new peaks at 26.3° and 33.2° appeared and were indexed to (0 5 0) and (2 0 0) planes. The changes in XRD spectra indicate that further crystallization of the BWO nanostructures occurred during calcination.

3.2. SEM and TEM investigations

The light absorption and photochemical reaction take place on solid surface of photocatalysts. Thus the surface microstructure plays key role in the photocatalytic process with respect to generation, transportation and reduction/oxidation of reactive species. To reveal the origin of the changes in photocatalytic activity of

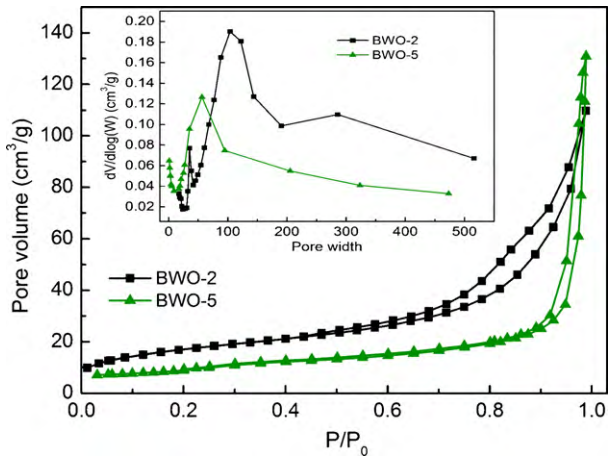

Fig. 4. Adsorption/desorption isotherms of the samples calcined at 200 °C and 500 °C.

the samples, the microstructure and crystal structure were further studied using SEM and TEM. Fig. 2a and b shows the SEM images of BWO-2 which appears a nanosheet self-constructed hierarchical porous structure. As observed in Fig. 2c and d, the nanosheets aggregated with each other and became looser after calcination at 500 °C. Additionally, Fig. 3a clearly shows that the nanosheet units of BWO-2 have irregular shape with many nanocrystals dispersed on them randomly. The nanocrystals possess a diameter of less than 10 nm and could be treated as quantum dots (QDS). Fig. 3b displays the HRTEM image of an isolated nanosheet of BWO-2. The fringes and the inset discontinuous FFT diffraction pattern show that the QDS and the nanosheet substrates are crystalline and they share a similar crystal orientation. Though several research groups have proposed possible formation mechanisms of BWO nanostructures [15–17], it is still not clear for our products considering the unique assembling units, neither just nanoparticles nor just single crystalline nanoplates. The difference may be closely related with different tungsten sources and the solvothermal reaction system. What is evident is that the calcination processing exerted a strong influence on BWO nanostructures. To provide more details of structure changes in calcination process, TEM and SAED analysis was also carried out on BWO-3 and BWO-4, which is shown in Fig. 3c and d. No distinct difference was observed between BWO-2 and BWO-3 while most QDS on the nanosheets disappeared when the sample was calcined at 400 °C. The SAED patterns of BWO-3 and BWO-4 in the inset of Fig. 3c and d also indicate the improvement of crystallinity. When heat treated at 500 °C, the single crystalline BWO nanoplates tended to became square, as is clearly displayed in the TEM image of Fig. 3e. Moreover, from Fig. 3f, the fringes became very clear and continuous, indicating the high degree of crystallinity, which was also confirmed by the inset corresponding FFT diffraction pattern. The above results demonstrate that the crystallinity of BWO nanostructured was improved after calcination, accompanied by the disappearance of BWO QDS [18].

3.3. Surface analysis

Surface area is another key structural parameter for photocatalysts. To determine surface area of the samples, surface analysis was carried out using nitrogen adsorption/desorption method. The isotherms of BWO-2 and BWO-5 are shown in Fig. 4a. From the figure, both isothermals were categorized as type II with a H4 hysteresis loop according to the IUPAC classifications, indicating a macroporous characteristic of BWO nanostructures with silt-like pores. Moreover, the hysteresis loop of BWO-5 shifts to right after calcination at 500 °C, indicating the amount of pores

Table 1
BET surface area of the calcined samples.

Sample	BWO-2	BWO-3	BWO-4	BWO-5
S_{BET} (m^2/g)	60.3	54.2	35.6	30.7

became less compared with that of BWO-2 [19]. The pore size distribution curves were obtained from Barrett–Joyner–Halanda (BJH) desorption branches. As is shown in the inset of Fig. 4, there was a peak concentrating at 100 nm for BWO-2 whereas for BWO-5, the peak appeared at around 60 nm, suggesting the silt-like pores between the nanosheets became smaller. The surface area of different samples determined by BET method was listed in Table 1. With increasing calcination temperature, the surface area of BWO nanostructures decreased by one half from 60.3 m^2/g to 30.7 m^2/g.

3.4. Optical properties

Fig. 5 shows the UV–vis spectra of the calcined samples. The absorbance spectra were converted from the reflection by Kubelka–Munk method [20]. From the figure, all the samples show god response to visible light. The BWO-2 and BWO-3 exhibited higher light absorption in the wavelength region longer than 438 nm. The optical band gap of the samples was also estimated based on their absorption spectra according to the following equation:

$$\alpha h\nu = A(E_g - h\nu)^n$$

where α, A, h, ν, E_g are the absorption coefficient, proportional coefficient, Plank constant, light frequency and band gap, respectively, while n describes the optical transition type of a semiconductor. The value of n for BWO is 2, which means that the optical transition is indirect allowed [21]. The estimated optical band gap decreased as the calcination temperature was raised. The optical band gap of BWO-2 was 2.76 eV larger than that of BWO-5, which could be ascribed to the quantum confinement effect that widened the band gap by forming discrete energy levels in semiconductor QDS [22].

3.5. Photocatalytic activity

Photocatalytic activity was evaluated by degradation of RhB under visible-light irradiation ($\lambda > 420$ nm). Fig. 6a shows the change in relative concentration of RhB with irradiation time using the calcined samples as photocatalysts. No obvious degradation of RhB was observed for both blank test and dark test, indicating the dyes was stable under visible-light irradiation and the adsorption of

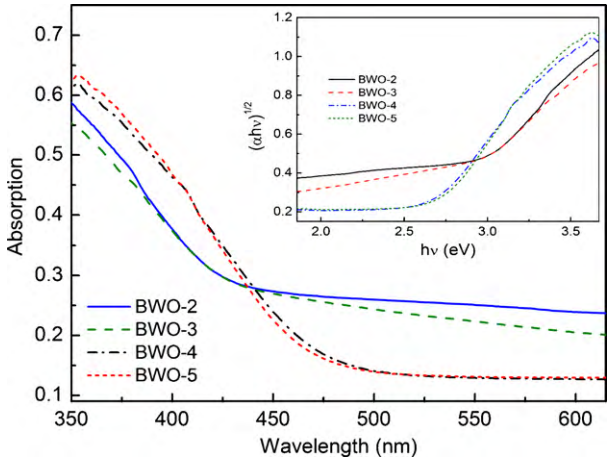

Fig. 5. UV–vis spectra of the calcined samples and the curves of $(\alpha h\nu)^{1/2}$ vs. $h\nu$.

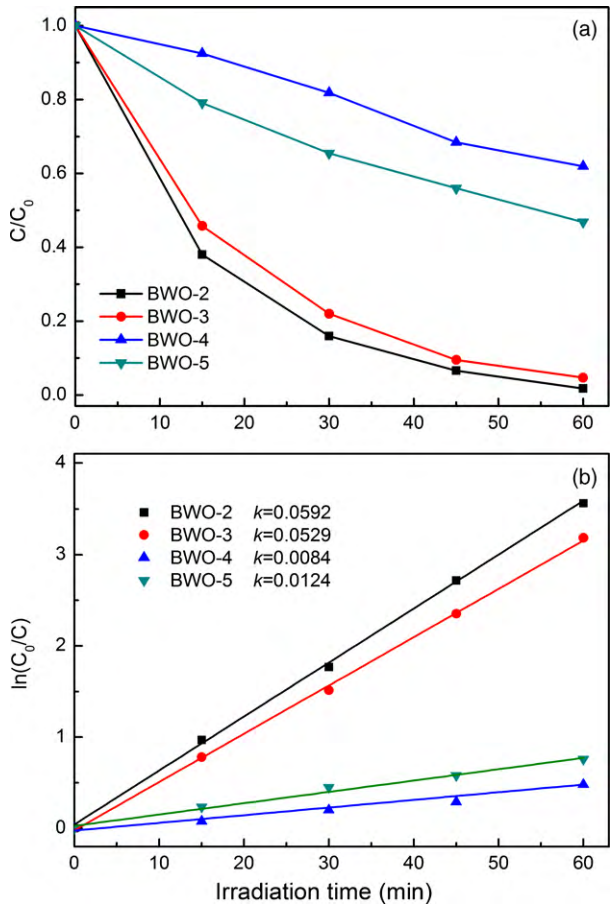

Fig. 6. Photocatalytic activity of the calcined samples (a) and the curves of $\ln(C_0/C)$ vs. irradiation time (b).

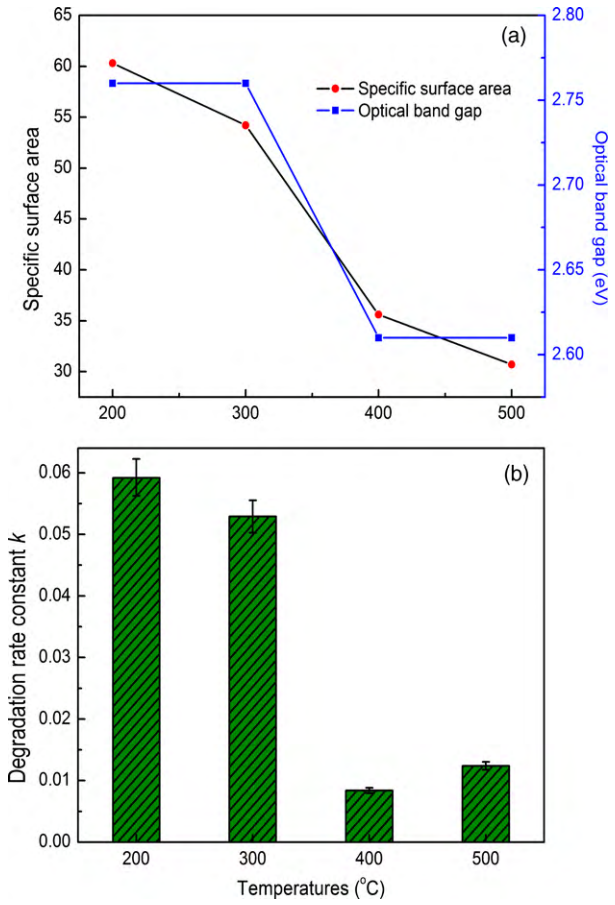

Fig. 7. Effects of calcination on surface area, optical band gap (a) and the photocatalytic efficiency (b) of the calcined samples.

RhB on the photocatalyst was negligible after reaching adsorption-desorption equilibrium. After 60 min, photocatalytic efficiency of BWO-2 reached almost 100%. The value dropped to 94% for BWO-3. Under the same conditions, only 41% and 52% of RhB was degraded for BWO-4 and BWO-5. The photochemical reaction was also fitted for pseudo-first-order kinetics. The reaction constant k which is used to evaluate the degradation rate could be determined from the plots of $\ln(C_0/C)$ vs. irradiation time. As is shown in Fig. 6b, the obtained k value was much higher for the samples calcined at lower temperature. The degradation rate for BWO-2 was almost five times the value for BWO-5.

3.6. *Processing–structure–property relationships*

The processing of calcination led to structure–property evolution of the BWO nanostructures and the effects of calcination on both the structure and the photocatalytic activity are shown in Fig. 7. With increasing calcination temperature, the nanosheets aggregated with each other due to thermal stress. Higher temperature calcination provided more energy to enhance the mobility of atoms, which could strengthen the crystallization effect. The Morphology of BWO nanosheets changed from irregular shape to square-like, which also confirmed the role of calcination in the crystallization process. Obviously, the crystallinity of BWO nanostructures was improved because of calcination, which means the concentration of defects in the crystal structure became lower and thereby the trapping of photogenerated carriers was greatly weakened [23]. However the photocatalytic activity of BWO nanostructures did not increased until the calcination temperature was promoted from 400 °C to 500 °C. Therefore, one more structural factor has to be taken into account. Surface area associates with light absorption and photochemical reaction place. Large surface area produces better light harvesting and more active sites for photochemical reaction [24]. The surface area of BWO nanostructures decreased with the step-rise calcination temperature. The decrease of surface area was partly due to the aggregation of nanosheets but mainly caused by the gradual disappearance of BWO QDS because the atoms on the BWO QDS were more active when calcined and they tended to migrate to BWO nanosheet substrates to reduce their large surface energy [25]. Recently, Amano evidenced the positive role of good crystallinity and large surface area for the photocatalytic materials [26,27]. In this case, the effect of crystallinity on the photocatalytic activity competed with that of surface area, i.e. the decrease of surface area accompanied by the increase of crystallinity during calcination. Based on the changes in structure and activity shown in Fig. 7, also considering the above XRD and TEM results, the calcination processing of BWO nanostructures could be classified into three categories. From 200 °C to 300 °C, the crystallinity changed only a little and the decrease in surface area made the photocatalytic activity drop to a certain extent; From 300 °C to 400 °C, the crystallinity tended to be improved and the surface area decreased a lot, which highlighted the important role of surface area in the photochemical reaction; From 400 °C to 500 °C, the crystallinity became very high and the surface area continued to decrease but not very much. The excellent crystallinity effectively lowered the combination probability of photogenerated carriers in the BWO nanostructures. That led to a slight increase of the photocatalytic efficiency. But those facts did not change the overall trend of structure–property evolution. That is, the calcination at higher temperature indeed

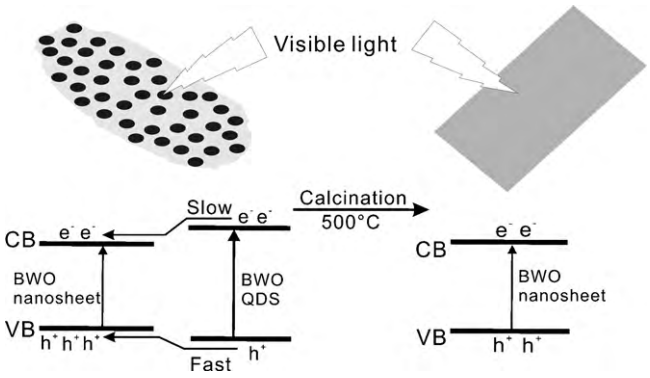

Fig. 8. Illustration of the transfer process of photogenerated carriers for the samples calcined at 200 °C and 500 °C.

brought down the photocatalytic activity of the BWO nanostructures.

Besides the most important structural factors of crystallinity and surface area, another factor that should be considered is the possible existence of semiconductor junction in the BWO nanostructures. As is known, one popular method to improve the activity of the photocatalysts is to couple two semiconductors [28]. There have been many reports on heterojunction of photocatalysts such as Co_3O_4/Bi_2WO_6 [29] and PbS/TiO_2 [30] whose role is to separate the photogenerated carriers and prolong their lifetime. However, only a few reports referred to homojunction of semiconductors. More recently, Yang et al. reported that the photocatalytic activity of TiO_2 could be enhanced by forming homojunction between the anatase TiO_2 and TiO_2 (B) which differed in band structure [31]. Similar electron transfer behavior also existed in the homojunction between the silicon QDS and silicon plates [32]. Inspired by that, it was reasonable to anticipate homojunctions between BWO QDS and BWO nanosheets. When BWO nanostructures were calcined at lower temperature, there exist many BWO QDS dispersed on BWO nanosheet substrates, and the similar crystal orientation indicates an intimate contact, which enables the formation of homojunctions. Moreover, the energy level of conduction band (CB) became higher and that of valence band (VB) became lower due to the quantum confinement effect, which made the generation and migration of photogenerated carriers different from that of the BWO nanostructures composed of only nanosheets at higher calcination temperature. Fig. 8 illustrates the transfer process of the photogenerated carriers for the samples of BWO-2 and BWO-5. When the QDS modified BWO nanostructures were exposed to visible light, the photogenerated electrons and holes migrated from BWO QDS to BWO nanosheet substrates. But generally, the migration rate of CB electrons is slower than that of VB holes [31], thus leaving more electrons in the CB of QDS. That means the separation of photogenerated carriers could be realized. But the separation mechanism was vitiated when the samples were calcined at higher temperatures such as 500 °C. Thereby, it was believed that the BWO QDS which were stable at lower calcination temperature not only contributed to the large surface area but also prolonged the lifetime of photogenerated carriers.

4. Conclusions

In summary, QDS modified BWO nanostructures synthesized by solvothermal method were processed by calcination from 200 °C to 500 °C. A strong correlation was found among the processing, structure and properties of the samples. With increasing calcination temperature, the crystallinity of the samples became higher and most QDS gradually disappeared from the BWO nanostructures. Both surface area and band gap of the samples decreased. The light absorption of the samples became lower for the long-wavelength range, accompanied by a red shift of the absorption edge. The competitive relations between crystallinity and surface area in affecting the photocatalytic activity were discussed. It was further proposed that the BWO QDS stable at lower calcination temperature not only contributed to the large surface area but also played a part in improvement of photocatalytic activity by facilitating the separation of photogenerated carriers. Our work reported here also demonstrates a new strategy for the design of nanostructured photocatalysts with high performance.

Acknowledgements

This work was supported by the National Basic Research Program of China (Grant No. 2009CB939705 and 2009CB939702), Nature Science Foundation of China (Grant No. 50772040 and 50927201) and the Opening Research Foundation of State Key Laboratory of Advanced Technology for Materials Synthesis and Processing (Wuhan University of Technology). Also, the technology was supported by the Analytic Testing Center of HUST for carrying out XRD and FESEM analysis.

References

[1] A. Fujishima, K. Honda, Electrochemical photolysis of water at a semiconductor electrode, Nature 238 (1972) 37–38.
[2] J.M. Herrmann, Heterogeneous photocatalysis: fundamentals and applications to the removal of various types of aqueous pollutants, Catal. Today 53 (1999) 115–129.
[3] M.D. Hernandez-Alonso, F. Fresno, S. Suarez, J.M. Coronado, Development of alternative photocatalysts to TiO_2: challenges and opportunities, Energy Environ. Sci. 2 (2009) 1231–1257.
[4] A. Kudo, H. Kato, Photocatalytic activities of $Na_2W_4O_{13}$ with layered structure, Chem. Lett. (1997) 421–422.
[5] H.B. Fu, J. Lin, L.W. Zhang, Y.F. Zhu, Photocatalytic activities of a novel $ZnWO_4$ catalyst prepared by a hydrothermal process, Appl. Catal. A Gen. 306 (2006) 58–67.
[6] D. Ye, D.Z. Li, W.J. Zhang, M. Sun, Y. Hu, Y.F. Zhang, X.Z. Fu, A new photocatalyst $CdWO_4$ prepared with a hydrothermal method, J. Phys. Chem. C 112 (2008) 17351–17356.
[7] J.W. Tang, Z.G. Zou, J.H. Ye, Photocatalytic decomposition of organic contaminants by Bi_2WO_6 under visible light irradiation, Catal. Lett. 92 (2004) 53–56.
[8] J.G. Yu, J.F. Xiong, B. Cheng, Y. Yu, J.B. Wang, Hydrothermal preparation and visible-light photocatalytic activity of Bi_2WO_6 powders, J. Solid State Chem. 178 (2005) 1968–1972.
[9] H.B. Fu, C.S. Pan, W.Q. Yao, Y.F. Zhu, Visible-light-induced degradation of rhodamine B by nanosized Bi_2WO_6, J. Phys. Chem. B 109 (2005) 22432–22439.
[10] X. Hu, G. Li, J.C. Yu, Design, Fabrication, and modification of nanostructured semiconductor materials for environmental and energy applications, Langmuir 26 (2009) 3031–3039.
[11] Z.G. Zhao, M. Miyauchi, Nanoporous-walled tungsten oxide nanotubes as highly active visible-light-driven photocatalysts, Angew. Chem. Int. Ed. 47 (2008) 7051–7055.
[12] Z.C. Shan, Y.M. Wang, H.M. Ding, F.Q. Huang, Structure-dependent photocatalytic activities of MWO_4 (M = Ca, Sr, Ba), J. Mol. Catal. A: Chem. 302 (2009) 54–58.
[13] J.H. Pan, H. Dou, Z. Xiong, C. Xu, J. Ma, X.S. Zhao, Porous photocatalysts for advanced water purifications, J. Mater. Chem. 20 (2010) 4512–4528.
[14] Z. He, C. Sun, S.G. Yang, Y.C. Ding, H. He, Z.L. Wang, Photocatalytic degradation of rhodamine B by Bi_2WO_6 with electron accepting agent under microwave irradiation: mechanism and pathway, J. Hazard. Mater. 162 (2009) 1477–1486.
[15] S.W. Liu, J.G. Yu, Cooperative self-construction and enhanced optical absorption of nanoplates-assembled hierarchical Bi_2WO_6 flowers, J. Solid State Chem. 181 (2008) 1048–1055.
[16] L.H. Zhang, W.Z. Wang, Z.G. Chen, L. Zhou, H.L. Xu, W. Zhu, Fabrication of flower-like Bi_2WO_6 superstructures as high performance visible-light driven photocatalysts, J. Mater. Chem. 17 (2007) 2526–2532.
[17] L.S. Zhang, W.Z. Wang, L. Zhou, H.L. Xu, Bi_2WO_6 nano- and microstructures: shape control and associated visible-light-driven photocatalytic activities, Small 3 (2007) 1618–1625.
[18] S.J. Xu, X.C. Wang, S.J. Chua, C.H. Wang, W.J. Fan, J. Jiang, X.G. Xie, Effects of rapid thermal annealing on structure and luminescence of self-assembled InAs/GaAs quantum dots, Appl. Phys. Lett. 72 (1998) 3335–3337.
[19] C.X. Xu, X. Wei, Z.H. Ren, Y. Wang, G. Xu, G. Shen, G.R. Han, Solvothermal preparation of Bi_2WO_6 nanocrystals with improved visible light photocatalytic activity, Mater. Lett. 63 (2009) 2194–2197.
[20] P. Kubelka, F. Munk, Ein beitrag zur optik der farbanstriche, Zeit. Tech. Phys. 12 (1931) 593–601.

[21] J.W. Tang, Z.G. Zou, J.H. Ye, Efficient photocatalysis on $BaBiO_3$ driven by visible light, J. Phys. Chem. C 111 (2007) 12779–12785.
[22] H. Weller, Quantized semiconductor particles: a novel state of matter for materials science, Adv. Mater. 5 (1993) 88–95.
[23] S. Rabindranathan, S. Devipriya, S. Yesodharan, Photocatalytic degradation of phosphamidon on semiconductor oxides, J. Hazard. Mater. 102 (2003) 217–229.
[24] A.G.S. Prado, L.L. Costa, Photocatalytic decouloration of malachite green dye by application of TiO_2 nanotubes, J. Hazard. Mater. 169 (2009) 297–301.
[25] L. Chen, Z.Q. Chen, X.Z. Shang, C. Liu, S. Xu, Q. Fu, Effect of annealing temperature on density of ZnO quantum dots, Solid State Commun. 137 (2006) 561–565.
[26] F. Amano, A. Yamakata, K. Nogami, M. Osawa, B. Ohtani, Visible light responsive pristine metal oxide photocatalyst: enhancement of activity by crystallization under hydrothermal treatment, J. Am. Chem. Soc. 130 (2008) 17650–17651.
[27] F. Amano, K. Nogami, M. Tanaka, B. Ohtani, Correlation between surface area and photocatalytic activity for acetaldehyde decomposition over bismuth tungstate particles with a hierarchical structure, Langmuir 26 (2010) 7174–7180.
[28] R. Khan, T.J. Kim, Preparation and application of visible-light-responsive Ni-doped and SnO_2-coupled TiO_2 nanocomposite photocatalysts, J. Hazard. Mater. 163 (2009) 1179–1184.
[29] Q. Xiao, J. Zhang, C. Xiao, X. Tan, Photocatalytic degradation of methylene blue over Co_3O_4/Bi_2WO_6 composite under visible light irradiation, Catal. Commun. 9 (2008) 1247–1253.
[30] C. Ratanatawanate, Y. Tao, K.J. Balkus, Photocatalytic activity of PbS quantum dot/TiO_2 nanotube composites, J. Phys. Chem. C 113 (2009) 10755–10760.
[31] D.J. Yang, H.W. Liu, Z.F. Zheng, Y. Yuan, J.C. Zhao, E.R. Waclawik, X.B. Ke, H.Y. Zhu, An efficient photocatalyst structure: TiO_2(B) nanofibers with a shell of anatase nanocrystals, J. Am. Chem. Soc. 131 (2009) 17885–17893.
[32] S. Park, E. Cho, X.J. Hao, G. Conibeer, M.A. Green, Study of silicon quantum dot p–n or p–i–n junction devices on c-Si substrate, commad: 2008, in: Conference on Optoelectronic and Microelectronic Materials & Devices, 2008, pp. 316–319.